TRANSPORT PROBLEMS 2018 Volume 13 Issue 2
PROBLEMY TRANSPORTU DOI: 10.20858/tp.2018.13.2.9

Keywords: aerodynamic noise; high-speed train; Lighthill-Curle theory; simulation model; on-line tests

Shi-jie JIANG*, Song YANG, Dan WU, Bang-Chun WEN
Northeastern University, School of Mechanical Engineering & Automation
Shenyang 110819, China
**Corresponding author*. E-mail: jiangsj@me.neu.edu.cn

PREDICTION AND VALIDATION FOR THE AERODYNAMIC NOISE OF HIGH-SPEED TRAIN POWER CAR

Summary. The aerodynamic noise of high-speed train power car was investigated in this article. The full-scale power car was first modeled, and the external steady flow field was computed by a realizable k-ε turbulence model. The aerodynamic noise sources of the power car surface and the external transient flow field were then calculated by broadband noise source model and large eddy simulation (LES) model, respectively. The static pressures on the train surface were obtained from the results of the transient model. Considering the transient flow field, the far-field aerodynamic noise generated by the power car was finally derived from Lighthill-Curle theory. It was validated by means of on-line tests that have been performed along a real high-speed railway line. Through comparisons between simulations and measurements, it is shown that the simulation model gives reliable aerodynamic noise predictions. We foresee numerous applications for modeling and control of the aerodynamic noise in high-speed train.

1. INTRODUCTION

High-speed trains are obviously superior to the conventional ones in terms of traveling speed, convenience, and comfort during any type of journey. They are also helpful to the economic development of urban and rural areas. However, high-speed railways inevitably bring some negative effects, one of which is noise. It mainly contains wheel/rail noise and aerodynamic noise [1, 2]. When a train is cruising at high speeds, normally above 250 km/h, aerodynamic noise becomes the dominant source [3, 4]. It not only seriously affects the passenger comfort and people's normal life along the railway line, but also may cause fatigue damage to the surrounding equipment and buildings, which greatly restricts the sustainable development of high-speed railways. Therefore, reducing aerodynamic noise is necessary and critical in order to promote high-speed railway transport and sustainability. For effective solutions, the dominant noise sources must be identified and the parameters that influence them should be understood before control implementations are made. Therefore, there is a requirement for the development of calculation method for prediction and insight into how the noise is generated [5-8].

At present, mainly two means are performed to study the flow and noise around a high-speed train: numerical and experimental research. About the numerical research [9-11], simulation technology of fluid dynamics has been widely utilized to study the aerodynamic noise of high-speed train. However, the relevant on-line tests are few; the past numerical research generally lacks validation. The existing experimental research is mostly carried out based on wind tunnel test [12-14], which investigates the characteristics of air flow and its interaction with the train scaling model in a wind tunnel. According to the similarity principle, the aerodynamic characteristics of a real train would be understood. However, the wind tunnel test is a kind of simulation test, and there are obvious limitations, such as boundary interference, holder interference, low Reynolds number, high cost, etc., which could

possibly result in inaccurate measurements. In this paper, the far field aerodynamic noise generated by high-speed train power car was predicted based on Lighthill-Curle theory [15-19] in FLUENT software. In addition, series of on-line tests were performed with a self-made test platform along a real high-speed railway line. Through the comparison between predictions and measurements, the simulation model was validated and the characteristics of the aerodynamic noise were obtained. This research provides the basis and technical support for simulation and control on the aerodynamic noise generated by a whole train (4 carriages together).

In this paper, simulation methodology and field measurement methods are introduced in Sections 2 and 3, respectively, followed by corresponding results and comparisons for validations in Section 4. Section 5 summarizes the conclusions.

2. SIMULATION METHODOLOGY

The simulation of the aerodynamic noise of high-speed train mainly includes: 1) calculating steady flow field by a realizable k-ε turbulence model, 2) simulating train surface noise sources by broadband noise source model, 3) obtaining the static pressures of the train surface based on the transient flow field calculated by the Large Eddy Simulation (LES) method, and 4) figuring out the far field aerodynamic noise of high-speed train power car by Lighthill-Curle theory with the transient flow field results.

2.1. 3D Modeling

A full-scale three-dimensional (3D) model was set up for the high-speed train power car (CRH380B type), with the length, width, and height being 25700 mm, 3400 mm, and 3700 mm, respectively. To improve the calculation efficiency, only windows, doors, and bogies were simplified, as shown in Fig. 1.

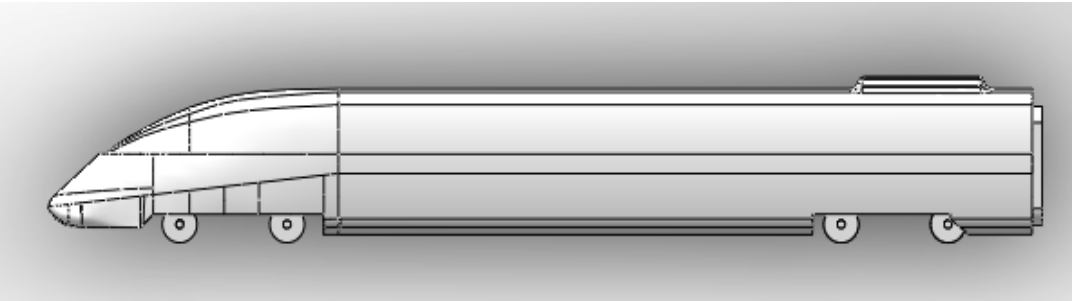

Fig. 1. 3D model of the train power car

To make sure that the flow field around the vehicle was not influenced, the external flow field boundary had to be large enough. Therefore, it was defined as a rectangle with 20 m height, and the distances are 30 m between its entrance boundary and the car front-end, 90 m between the exit boundary and the rear-end, and 20 m between the lateral boundary and the central line of the car, as shown in Fig. 2. Since the train is symmetric, only half of the model was analyzed to further improve the simulation efficiency.

The hybrid grid method was adopted to mesh the model, with the train meshed with triangle and quadrilateral elements and the external flow field meshed with tetrahedron (primary) and hexahedron (auxiliary) elements. The total number of mesh is about five million. Details are shown in Fig. 3.

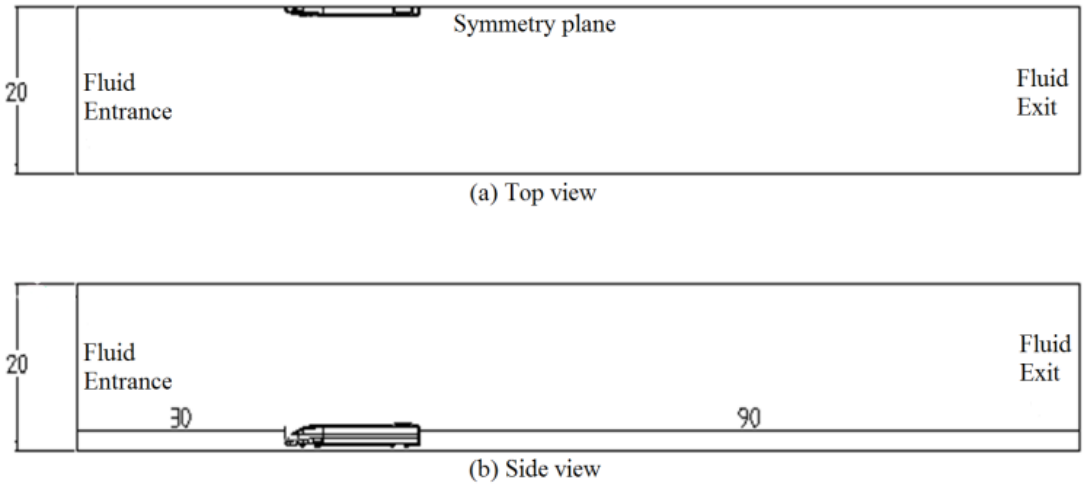

Fig. 2. Fluid field

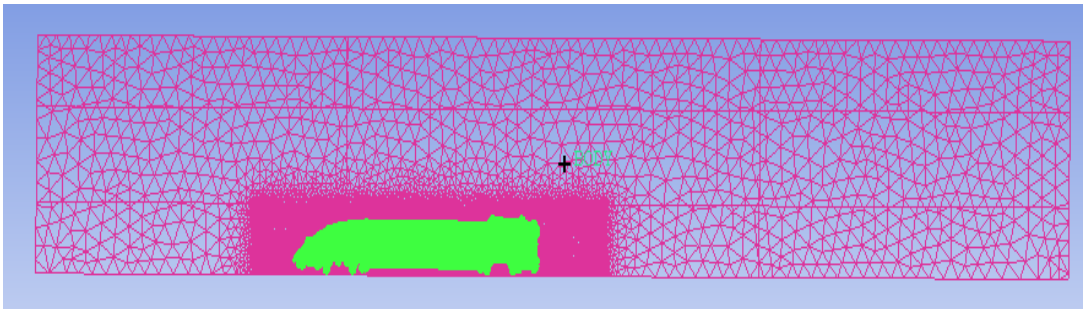

Fig. 3. Mesh structure of the vehicle and flow field

2.2. Steady state simulation

At present, the train speed is far lower than the sound speed and the Mach number is far less than 1, therefore, the surrounding air can be regarded as incompressible viscous fluid, the basic control equations are as follows:

$$\frac{\partial u_i}{\partial x_i} = 0 \tag{1}$$

$$\partial u_i + u_j \frac{u_i}{x_j} = -\frac{1}{\rho}\frac{\partial p}{\partial x_i} + \frac{\mu}{\rho}\frac{\partial^2 u_i}{\partial x_j x_j} \tag{2}$$

where u is the velocity component of the fluid (air) surrounding the train, x_i and x_j are position vectors (rectangular coordinate component), ρ and p are the density and pressure of the surrounding flow field, and μ is the air dynamic viscosity coefficient.

The turbulence flow could be described by the Navier-Stokes (N-S) equation, and the steady state calculation was carried out based on the realizable k-ε model [20]. This model is suitable for various types of flow (like spin uniform shear flow, channel flow, and boundary layer flow, etc.), and the simulation results are reliable. The model is based on the transport equations of the two variables, i.e. the turbulence kinetic energy (k) and the dissipation rate (ε), respectively. The equations are defined as follows:

$$\frac{\partial(\rho k)}{\partial t} + \frac{\partial(\rho k u_i)}{\partial x_i} = \frac{\partial}{\partial x_j}\left[\left(\mu + \frac{\mu_t}{\sigma_k}\right)\frac{\partial k}{\partial x_j}\right] + G_k + G_b - \rho\varepsilon \tag{3}$$

$$\frac{\partial(\rho\varepsilon)}{\partial t} + \frac{\partial(\rho\varepsilon u_i)}{\partial x_i} = \frac{\partial}{\partial x_j}\left[\left(\mu + \frac{\mu_t}{\sigma_\varepsilon}\right)\frac{\partial k}{\partial x_j}\right] + \rho C_1 E\varepsilon - \rho C_2 \frac{\varepsilon^2}{k+\sqrt{\gamma\varepsilon}} + C_{1\varepsilon}\frac{\varepsilon}{k}C_{3\varepsilon}G_b \tag{4}$$

where G_k represents the turbulence kinetic energy generated by average velocity gradient, G_b is the turbulence kinetic energy generated by buoyancy, σ_k is a constant, $\sigma_k = 1.0$, σ_ε is the Prandtl number for the turbulence kinetic energy dissipation rate, $\sigma_\varepsilon = 1.2$, E is the source term, $C_1 = \max\left[0.43, \frac{\eta}{\eta+5}\right]$, $\eta = \mathrm{S}\frac{k}{\varepsilon}$, $\mathrm{S} = \sqrt{2}S_{\mathrm{ij}}$, S_{ij} is the stress rate tensor. The main parameters settings in the steady state flow field simulation are shown in Table 1.

Table 1

Steady state flow field simulation settings

Category	Contents	Setup
General	Solver Type	Pressure-Based
	Time	steady
Models	k-epsilon	Realizable
Materials	air	
	Inlet	Velocity inlet U=83.3m/s k=0.2604m^2/s^2 ε=0.0273m^2/s^3
Boundary Conditions	Outlet	Pressure outlet
	Ground	wall
	Fluid domain surface	Symmetry
	Fluid domain	Interior
Run Calculation	Number of Iterations	2000

2.3. Aerodynamic noise source calculation

Ignoring the differential of time delay (replaced by covariance equivalent synchronization), Proudman [21] obtained the radiated acoustic power P_A of isotropic turbulence per unit volume deduced by Acoustic analogy theory under the condition of low Mach number and high Reynolds number, the expression is:

$$P_A = \alpha\rho_0\left(\frac{U^3}{l}\right)\frac{U^5}{c_0^5} \tag{5}$$

where ρ_0 is the average fluid density without disturbance, l is the turbulence length, c_0 is sound speed, α is a model constant. In the form of k and ε, it can be expressed as $P_A = \alpha_\varepsilon\rho_0\varepsilon M_t^5$, and $M_t = \sqrt{2k}/c_0$.

Sarker and Hussaini [22] calculated the isotropic turbulence with the direct numerical simulation method, obtaining 0.1 for α_ε. On the basis of the steady state calculation of the turbulence model, the turbulence kinetic energy and dissipation rate of each node in the flow field were extracted, and the sound power of each node was obtained, with which the distribution of the sound power level on the vehicle surface was worked out.

2.4. Transient state simulation

Transient state calculation was performed by the LES model [16], whose core meaning is that filtering the vortices less than a certain scale in the transient flow field, then the rest of the large eddies could be obtained by N-S equations. They are expressed as:

$$\frac{\partial\rho}{\partial t} + u\frac{\partial\rho\overline{u_i}}{\partial x_i} = 0 \tag{6}$$

$$\frac{\partial}{\partial t}(\rho\overline{u_i}) + \frac{\partial}{\partial x_j}\left(\rho\overline{u_i u_j}\right) = \frac{\partial}{\partial x_j}\left(u\frac{\partial\overline{u_i}}{\partial x_j}\right) - \frac{\partial\bar{p}}{\partial x_j} - \frac{\partial\tau_{ij}}{\partial x_j} \tag{7}$$

where $\overline{(\ )}$ is the spatial filtering, t is time, τ_{ij} is the sub grid-scale stress, $\tau_{ij} = \rho\overline{u_i u_j} - \rho\overline{u_i}\,\overline{u_j}$, which embodies the effect of small-scale eddies on the equation of motion. The main parameter settings in the transient flow field simulation are shown in Table 2.

Table 2

Transient state simulation settings

Category	Contents	Setup
General	Solver Type	Pressure-Based
	Time	Transient
Models	LES	
Materials	air	
Boundary Conditions	Inlet	Velocity inlet U=83.3 m/s k=0.2604 m^2/s^2 ε=0.0273 m^2/s^3
	Outlet	Pressure outlet
	Ground	wall
	Fluid domain surface	Symmetry
	Fluid domain	Interior
Run Calculation	Number of Iterations	4000

2.5. Far-field aerodynamic noise simulation

The far-field aerodynamic noise of high-speed train was simulated by Acoustic analogy method deduced by Lighthill [18, 19] based on Navier-Stokes (N-S) equation and continuity equation. The sound propagation can be expressed as

$$\frac{\partial^2 \rho'}{\partial t^2} - c_0^2 \nabla^2 \rho' = \frac{\partial^2 T_{ij}}{\partial x_i \partial x_j} \tag{8}$$

where T_{ij} is Lighthill turbulence stress tensor, $T_{ij} = \rho v_i v_j + \delta_{ij}[(p - p_0) - c_0^2(\rho - \rho_0)] - e_{ij}$, ρ_0 and p_0 are the average fluid density and pressure without disturbance, e_{ij} is the fluid viscous stress tensor, ρ' and p' are the fluctuating values of fluid density and pressure, and $\rho' = \rho - \rho_0$, $p' = p - p_0$.

When there is a solid wall boundary in unsteady flow field, the solution to Lighthill equation deduced by Curle yields:

$$\rho'(x,t) = \frac{1}{4\pi c_0^2}\left[\frac{\partial^2}{\partial x_i' x_j'}\int_v \frac{T_{ij}(y, t - R/c_0)}{R}\,dy - \frac{\partial}{\partial x_i'}\int_S \frac{n_j P_{ij}(y, t - R/c_0)}{R}\,dy\right] \tag{9}$$

where n_j is the cosine of the outward direction (pointing to the fluid) perpendicular to the solid wall, P_{ij} is the fluctuating pressure on the vehicle surface, y is the sound source point vector, x is the receiver point vector, $R = x - y$.

There are two types of noise source included in Equation (9): the first term of the right hand side is dipole noise source (derived from the Lighthill stress of the flow field around the vehicle) and the other one is quadrupole source (from the vehicle's surface pressure and viscous shear stress). Since the dipole source noise and quadrupole source noise are respectively proportional to the third power and fifth power of Mach number, the ratio of the quadrupole source noise to the dipole source noise is proportional to the square of Mach number. As the Mach number of the vehicle is about 0.245 under the present running speed (around 300 km/h), the quadrupole source noise is relatively smaller, and it can be ignored. Therefore, the formula for calculating the aerodynamic noise of high-speed train can be expressed as

$$\rho'(x,t) = -\frac{1}{4\pi c_0^2}\frac{\partial}{\partial x_i'}\int_S \frac{n_j P_{ij}(y, t - R/c_0)}{R}\,dy \tag{10}$$

$$P(x,t) - P_0 = c_0^2 \rho'(x,t) \tag{11}$$

where P is sound pressure, and P_0 is the reference sound pressure, $P_0 = 2 \times 10^{-5}$Pa.

According to the results of the transient state simulation, the fluctuating pressure of each node on the vehicle surface can be extracted, based on which the far-field aerodynamic noise pressures of high-speed train could be worked out with Equations (10) and (11).

3. ON-LINE TEST

At present, the high-speed railways are generally built on viaducts, in order to avoid foundation settlement, ensure safety, reduce cost and so on. The railways height could be up to 11 meters, and they are mostly far away from the urban area with complex terrains. These cause it difficult to directly measure the aerodynamic noise of high-speed train. In this paper, series of on-line tests have been performed along a high-speed railway line using a self-designed aerodynamic noise collection platform, mainly including microphone (BSWA-MP201), NI USB-4431 data acquisition card, tachymeter (Bushnell 101921), etc., as shown in Fig. 4. When the train (CRH380B) was passing by, the real-time signal (like noise and speed) was recorded. Two microphones were positioned to receive aerodynamic noise at different heights, and one was 7.5 m from the railway central line (according to ISO 3095:2005) and 3.5 m above the rail head and the other was the same length from the railway central line but 1.5 m above the rail head, as shown in Fig. 5. Compared with wind tunnel test, the on-line test is more accurate and cost saving.

(a) Tachymeter (b) Laser rangefinder (c) Noise collection system

Fig. 4. On-line test equipment

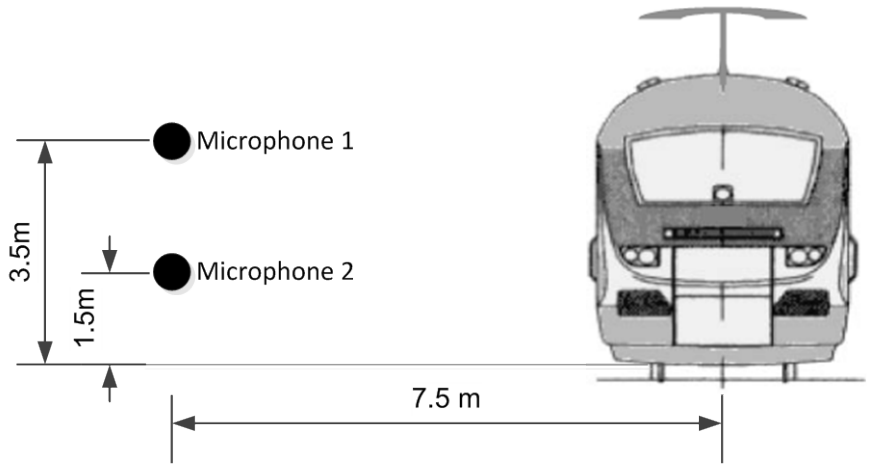

Fig. 5. Monitoring points for measuring aerodynamic noise

4. RESULTS AND DISCUSSION

At the vehicle head, the flow was divided into three parts and flowed over the vehicle surface, one flowed to the roof, one to the wall, and another to the bottom. Owing to the complexity of the bogie, the fluid flow was complicated and vortex occurs as shown in Fig. 6. While at the rear end of the vehicle, the mutual influence of vehicle's surface and ground effect with the effect of air viscosity causes vortex occurring again, as shown in Fig. 7. X-Z plane of the train was displayed, of which X is the horizontal direction and Z is the vertical direction. The wake flow structure of the vehicle shows the integrated effect of separation and interaction of each part of the vehicle.

As shown in Fig. 8, a positive pressure area occurs at the train head with a large gradient due to the area compressed by air, and the positive pressure is up to 4220Pa. The joint between the front window and the car body is nonstreamlined, which results in relatively high positive pressure (up to 2240 Pa). Since the curvature of the transition from train head to body changes obviously, the flow speed of the fluid becomes higher and its direction is to the inclined top of the train. It causes vacuum around the car body, and the positive pressures decreases to negative pressures, with the negative pressure down to −1710Pa, appearing on the top and side chamber surfaces of the transition from the train head to the body. Because of the extremely irregular shape of the bogie (at the bottom of the vehicle), the turbulence flow is complex and the intensity is high, causing the highest positive pressure, which is 5210 Pa.

From Fig. 9, it can be seen that there are corresponding trends in source power levels that are attributed to the changed static pressures as shown in Fig. 8. This confirms the consistence with Equations (10) and (11). Since the positive pressures at the areas of train head and front window are high, the corresponding aerodynamic noise is high. On the top and side chamber surfaces of the transition from the train head to the body, the negative pressure becomes maximum due to the interaction between vehicle surface and the external flow field, noise levels are relatively high. The surface of the vehicle body is smooth, with small curvature changes, the fluid flow is stable and noise levels are relatively low; while the sound power levels generated by the bogie are the highest, and it is because the bogie's shape is extremely irregular that results in severe and complicated turbulence flow.

To investigate the measurement of aerodynamic noise of the real vehicle passing by, the effects of environmental background noise have to be taken into account. Therefore, to ensure the accuracy, 20 groups of the real-time aerodynamic noise of high-speed train were measured, as well as 5 groups of background noise without trains passing by. Fig. 10 shows one example of the comparison between aerodynamic noise and background noise in time domain [23].

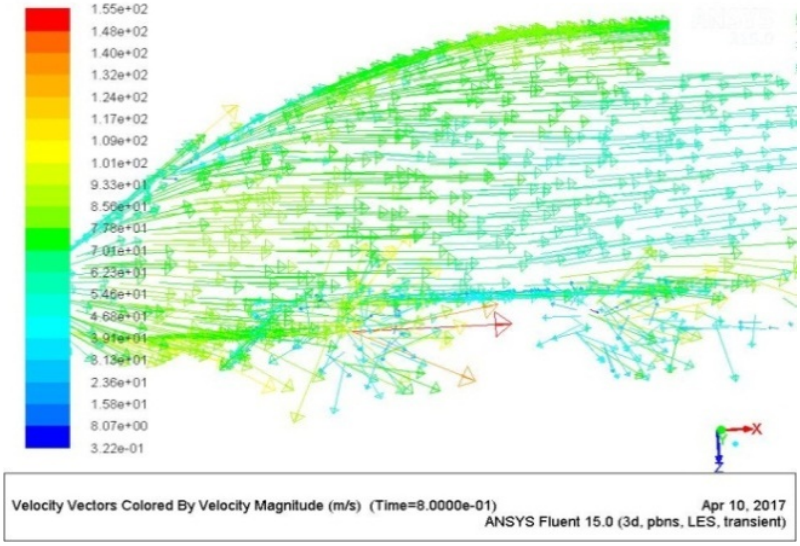

Fig. 6. Velocity vectors around train head

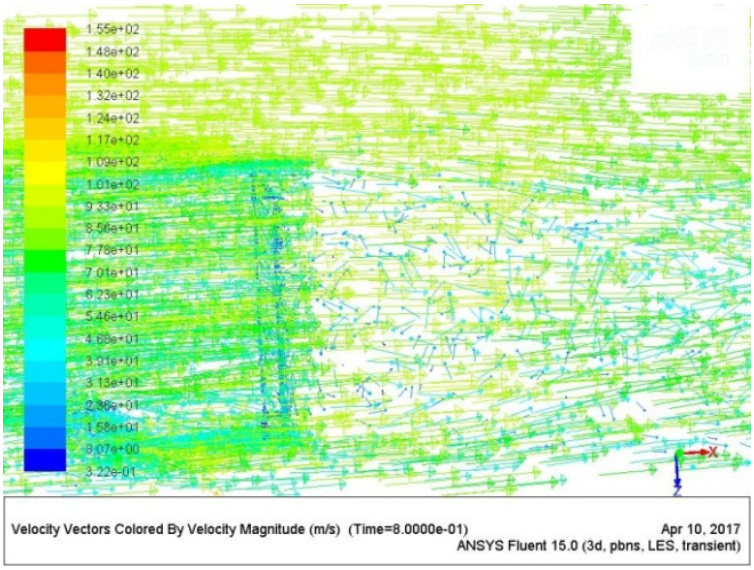

Fig. 7. Velocity vectors around train trail

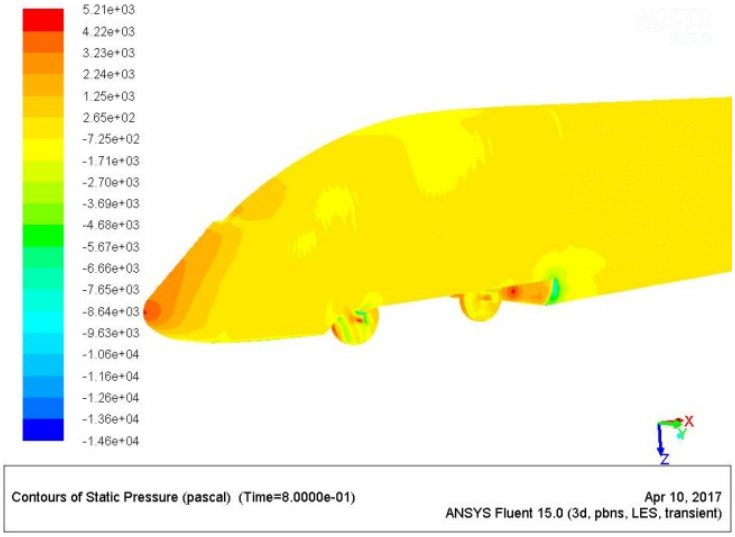

Fig. 8. Static pressure chart of the train head

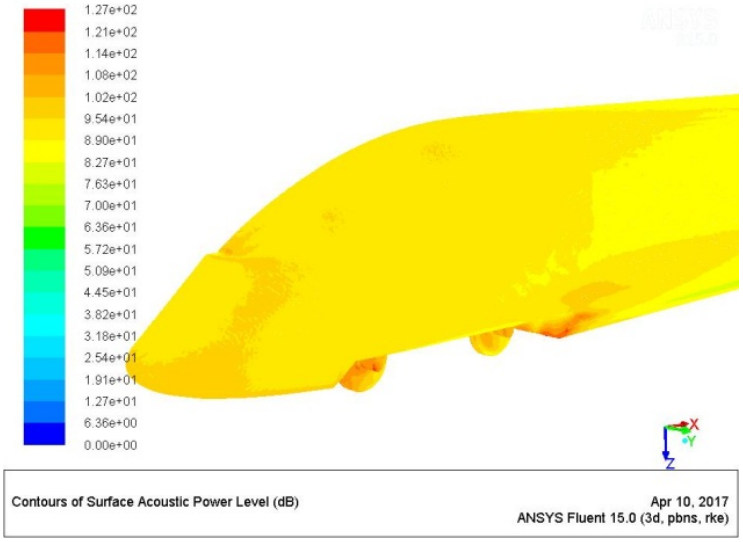

Fig. 9. Noise source power level chart of the train head

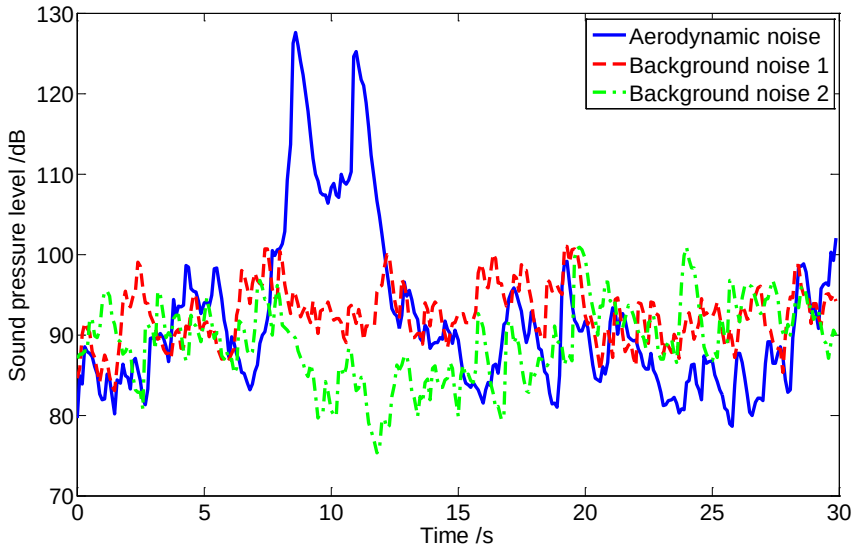

Fig. 10. Comparison in sound pressure level SPL between aerodynamic noise and background noise

From Fig. 10, it can be seen that the aerodynamic noise is significantly higher than the background noise. According to the principle of noise superposition $L = 10\lg\left(10^{L_1/10} + 10^{L_2/10} + \cdots + 10^{L_N/10}\right)$, if the difference between two noise sources in sound pressure level is more than 10dB, the source with larger SPL can be the result of superposition (with the deviation less than 0.4 dB). In addition, the train speed is about 300 km/h in this paper, the aerodynamic noise becomes the dominant noise source, and it is much larger than wheel/rail noise in SPL [4]. Therefore, both the wheel/rail noise and background noise can be ignored. Besides, the maximum SPL is mainly generated by the head of the power car, and the car body contributes less to the maximum value due to the smooth surface, therefore, it is possible to compare the simulations with the measurements to validate the simulation model for the high-speed train power car.

To compare the simulations with the on-line measurements, two monitoring points were chosen in the flow field. They were set at the same locations as those in on-line tests (shown in Fig. 5), simulating the received far-field aerodynamic noise. The comparisons between simulations and measurements in A-weighted SPL are shown in Figs. 11 and 12.

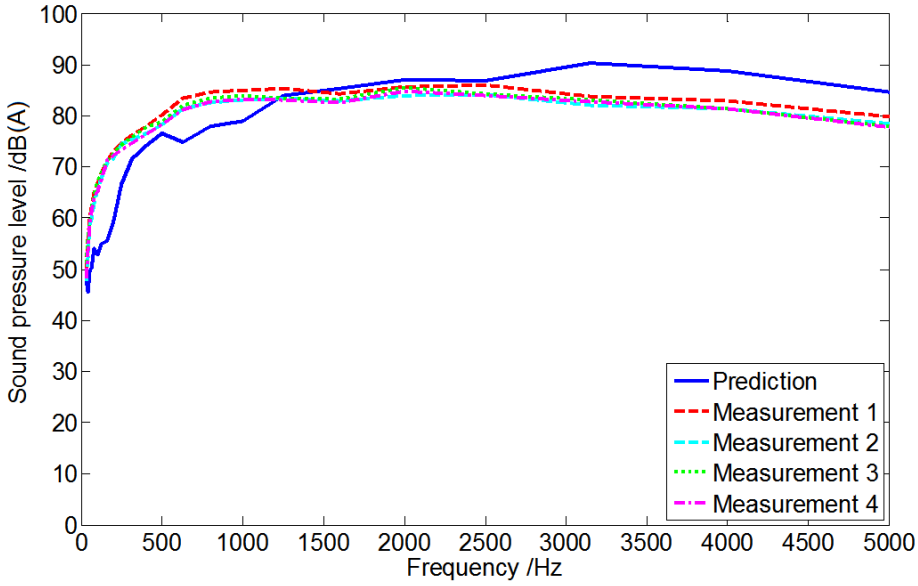

Fig. 11. 1/3 octave band A-weighted SPL at Monitor 1

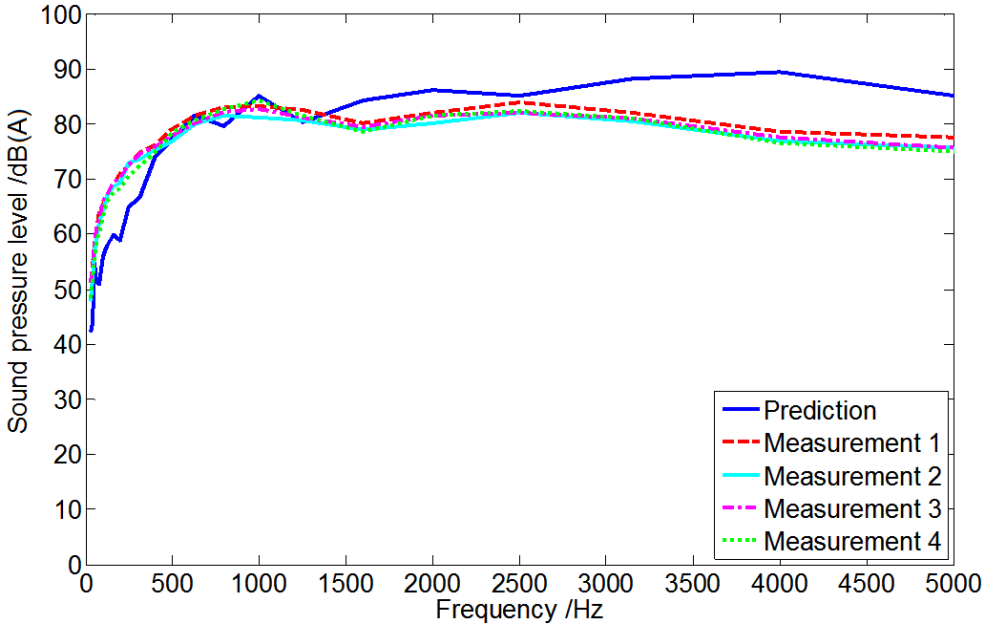

Fig. 12. 1/3 octave band A-weighted SPL at Monitor 2

According to Figs. 11 and 12, it can be seen that the aerodynamic noise of high-speed train is a type of broadband noise, i.e. there is no obvious frequency, and the noise energy is continuously distributed in a wide frequency scope (0-5000 Hz). In the frequency range from 500 Hz to 2500 Hz, the simulation results have a good agreement with the measurements. While below 500 Hz, there are slight under-predictions (less than 10%), this might be due to the simplification of doors, windows and bogies, where there could have been severe turbulence flows that could increase the noise levels. Above 2500 Hz, there are slight over-predictions (less than 10%), this might be because in the simulation, the ground was set as the solid wall that completely reflected the incoming noise without any attenuation, while in the experiment, the ground could absorb some noise energy, decreasing the noise levels received. In general, the simulations agree well with the measurements, and the simulation model is reliable.

5. CONCLUSIONS

In this paper, the full-scale 3D model of the high-speed train (CRH380B) power car was first set up, simulations on the aerodynamic noise were then carried out. The predictions were compared with the measurements, and the detailed conclusions are as follows:

1. The high positive pressures are mainly distributed at the parts of head and bogies. The negative pressures are distributed at the transition from train head to body. Vortex occurs at bogies and the rear end of the vehicle.
2. The aerodynamic noise generated by the bogie is the highest, followed by the nose part. The vehicle body produces far less noise and no obvious changes appear.
3. The aerodynamic noise of high-speed train is a type of broadband noise, i.e. there is no obvious frequency, and the noise energy is continuously distributed in a wide frequency scope (0-5000 Hz).
4. The simulations generally agree well with the measurements, and the simulation model is reliable.

Acknowledgement

The work described has been supported by the fundamental research funds for the central universities (N150303003) and research initiation funds for the PhD of Liaoning Province (201601005). Yihan Zhang and Yinfang Shi are also greatly appreciated for their assistance in doing field tests.

References

1. Sassa, T. & Sato, T. & Yatsui, S. Numerical Analysis of Aerodynamic Noise Radiation from a High-speed Train Surface. *Journal of Sound and vibration.* 2001. Vol. 247. P. 407-416.
2. Liu, J. The Theoretical Research and Numerical Simulation of Aerodynamic Noise of High-speed train. Master Dissertation. *Vehicle and Operation Engineering.* Southwest Jiaotong University 2009.
3. Zhu, J. & Hu, Z. & Thompson, D.J. Analysis of aerodynamic and aeroacoustic behaviour of a simplified high-speed train bogie. Presented at: *The 11th International Workshop on Railway Noise*. Chalmers. SE, 2013.
4. Yang, W. & Kim, D. & Park, J. & Koh, H. Analysis on the aeroacoustic sound radiation from high-speed train using a simplified numerical model. Presented at: *The 20th International Congress on Sound and Vibration* 2013. ICSV 2013. Bangkok, Thailand, 2013.
5. Raghunathan, R.S. & Kim, H.-D. & Setoguchi, T. Aerodynamics of high-speed railway train. *Progress in Aerospace Sciences.* 2002. Vol. 38. P. 469-514.
6. Parizet, E. & Hamzaoui, N. & Jacquemoud J. Noise assessment in a high-speed train. *Applied Acoustics.* 2002. Vol. 63. P. 1109-1124.
7. Liu J. Study on Chacteristics Analysis and Control of Aero-acoustics of High-speed Trains. Doctoral Dissertation. *Vehicle and Operation Engineering.* Southwest Jiaotong University. 2013.
8. I. M, M. T, & M. K. Development of low aerodynamic noise pantograph for high speed train. *Proceedings of International Congress Noise Control Engineering.* 1994. Vol. 1. P. 169-178.
9. Lyu, B. & Dowling, A.P. & Naqavi, I. Prediction of installed jet noise. *Journal of Fluid Mechanics.* 2016. Vol. 811. P. 234-268.
10. Liu, X. & Thompson, D. & Hu, Z. & Jurdic, V. Aerodynamic noise from a train pantograph, in *The 21st International Congress on Sound and Vibration*. Beijing. China. 2014.
11. Yoshiki, K. & Yusuke, W. & Fumio, M. & e. al, Numerical simulation of aerodynamic noise from high-speed pantographs using Lattice Boltzmann Method, presented at the *The International Symposium on Speed-up, Safety and Service Technology for Railway and Maglev Systems.* Seoul, Korea, 2012.
12. Muñoz-Paniagua, J. & García, J. & Crespo, A. Genetically aerodynamic optimization of the nose shape of a high-speed train entering a tunnel, *Journal of Wind Engineering and Industrial Aerodynamics.* 2014. Vol. 130. P. 48-61.
13. Gilbert, T. & Baker, C. J. & Quinn, A. Gusts caused by high-speed trains in confined spaces and tunnels. *Journal of Wind Engineering and Industrial Aerodynamics.* 2013. Vol. 121. P. 39-48.
14. Ricco, P. & Baronb, A. & Molteni P. Nature of pressure waves induced by a high-speed train travelling through a tunnel. *Journal of Wind Engineering and Industrial Aerodynamics.* 2007. Vol. 95. P. 781-808.
15. Williams, J. E. F. & Hawkings, D. L. So und Generation by Turbulence and Surfaces in Arbitrary Motion. *Philosophical Transactions of the Royal Society of London.* 1969. Vol. 264. P. 321-342.
16. Powell, A. Theory of Vortex Sound. *The Journal of Acoustical Society America.* 1964. Vol. 36. P. 177-195.
17. Curle, N. The Influence of Solid Boundaries upon Aerodynamic Sound. *Proceedings of the Royal Society of London.* 1955. Vol. 231. P. 506-514.
18. Lighthill, M.J. On Sound Generated Aerodynamically: Part II: Turbulence as a Source of Sound, *Proceedings of the Royal Society of London.* 1954. P. 1-32.
19. Lighthill, M.J. On Sound Generated Aerodynamically: Part I: General Theory, *Proceedings of the Royal Society of London.* 1952. Vol. 211. P. 564-587.
20. Zheng, Z. A Study on the Numerical Simulation of High-speed Vehicle's External Aerodynamic Acoustics Field. Doctoral Dissertation. *Vehicle Engineering.* Southwest Jiaotong University, 2012.
21. Proudman, I. & Pearson, J.R.A. Expansions at small Reynolds numbers for the flow past a sphere and a circular cylinder. *Journal of Fluid Mechanics.* 2006. Vol. 2. P. 237.

22. Sarkar, S. & Erlebacher, G. & Hussaini, M.Y. & H. O. Kreiss. The analysis and modelling of dilatational terms in compressible turbulence. *Journal of Fluid Mechanics.* 2006. Vol. 227. P. 473-493.
23. Deng, Y. Q. & Xiao, X.B.& He, B. & Jin, X.S. Analysis of external noise spectrum of high-speed railway. *Journal of Central South University.* 2014. Vol. 21. P. 4753-4761.

Received 09.11.2016; accepted in revised form 08.06.2018